energies

MDPI

Article

Thermodynamic Evaluation of the Hybrid Combined Cycle Power Plant in the Valley of Mexico

Ladislao Eduardo Méndez-Cruz [1,2], Martín Salazar-Pereyra [1], Raúl Lugo-Leyte [3], Mauricio Sales-Cruz [2], Alejandro Torres-Aldaco [3] and Helen D. Lugo-Méndez [2,*]

[1] División de Ingeniería Mecatrónica e Industrial, Tecnológico Nacional de México/TES de Ecatepec, Av. Tecnológico S/N, Col. Valle de Anáhuac, Ecatepec de Morelos 55210, Mexico; lemc@tese.edu.mx (L.E.M.-C.); msalazar@tese.edu.mx (M.S.-P.)

[2] Departamento de Procesos y Tecnología, Universidad Autónoma Metropolitana—Cuajimalpa, Av. Vasco de Quiroga No. 4871, Colonia Santa Fé, Cuajimalpa, Mexico City 05348, Mexico; asales@cua.uam.mx

[3] Departamento de Ingeniería de Procesos e Hidráulica, Universidad Autónoma Metropolitana—Iztapalapa, Av. Ferrocarril San Rafael Atlixco No. 186, Colonia Leyes de Reforma 1ª Sección, Iztapalapa, Mexico City 09340, Mexico; lulr@xanum.uam.mx (R.L.-L.); ata@xanum.uam.mx (A.T.-A.)

* Correspondence: hlugo@cua.uam.mx

Abstract: Modern power generation aims to maximize the extraction of thermal energy from fossil fuels to produce electricity. Combined cycle power plants, leaders in efficiency, sometimes require an additional steam generator to compensate for insufficient exhaust gas energy in the heat recovery steam generator (HRSG), leading to hybrid combined cycles. This study presents a comprehensive thermodynamic analysis of the hybrid combined cycle power plant located in the Valley of Mexico, operating under both full-load and partial-load conditions. The investigation begins with an energy analysis evaluating key performance parameters under real operating conditions, including the power generation, heat flow supply, thermal efficiency, fuel consumption rates, steam flow, and specific fuel consumption. Subsequently, the analysis examines the performance of the steam cycle using the β factor, which quantifies the relationship between heat flows in the steam generator and the HRSG, to maintain a constant steam flow. This evaluation aims to determine the potential utilization of exhaust gas residual energy for partial steam flow generation in the steam turbine. The study concludes with an exergy analysis to quantify the internal irreversibility flows within the system components and determine the overall exergy efficiency of the power plant. The results demonstrate that, under 100% load conditions, the enhanced utilization of exhaust gases from the HRSG leads to fuel savings of 33,903.36 tons annually and increases the exergy efficiency of the hybrid combined cycle power plant to 54.08%.

Keywords: thermodynamic analysis; hybrid combined cycle; power output; exergetic efficiency; irreversibility flows

check for updates

Academic Editor: Andrea De Pascale

Received: 6 March 2025
Revised: 1 April 2025
Accepted: 4 April 2025
Published: 9 April 2025

Citation: Méndez-Cruz, L.E.; Salazar-Pereyra, M.; Lugo-Leyte, R.; Sales-Cruz, M.; Torres-Aldaco, A.; D. Lugo-Méndez, H. Thermodynamic Evaluation of the Hybrid Combined Cycle Power Plant in the Valley of Mexico. *Energies* **2025**, *18*, 1901. https://doi.org/10.3390/en18081901

Copyright: © 2025 by the authors. Licensee MDPI, Basel, Switzerland. This article is an open access article distributed under the terms and conditions of the Creative Commons Attribution (CC BY) license (https://creativecommons.org/licenses/by/4.0/).

1. Introduction

The unprecedented and growing global demand for electricity has accelerated the depletion of natural resources, increased production costs, and exacerbated environmental degradation. This situation underscores the need to implement hybrid solutions that combine conventional and renewable energy sources to meet demand more efficiently and sustainably. While international policies increasingly promote renewable energy technologies, particularly solar and wind systems, fossil fuels continue to dominate global

power generation portfolios. Within this conventional energy framework, various technological configurations address growing energy demands: subcritical, supercritical, and ultra-supercritical thermal plants, standalone gas turbines, and combined cycle power plants (CCPPs) [1,2]. CCPPs have distinguished themselves through exceptional thermal efficiencies reaching 65%, integrating gas turbine cycles for primary power generation with heat recovery steam generators (HRSGs) that capture exhaust gas thermal energy to produce steam for additional electricity generation.

Therefore, CCPP technology plays a crucial role in the study and enhancement of power generation performance. In this regard, numerous studies have addressed energy and exergy analyses, examining various configurations of both the gas turbine cycle and the steam cycle. Shireef et al. conducted a thermodynamic analysis of a triple-pressure combined cycle, determining an exergy efficiency of 54%. They also identified the combustion chamber as the component contributing most significantly to exergy destruction. Furthermore, they demonstrated that increasing the live steam pressure in the steam cycle can enhance the combined cycle's power output [3].

On the other hand, Kotowicz et al. showed that a triple-pressure CCPP can achieve a thermal efficiency of up to 65% through the implementation of a gas turbine with sequential combustion [4]. Aliyu et al. focused on evaluating the performance of a combined cycle by analyzing the operational parameters of the steam cycle. They determined that live steam pressure, reheat pressure, and steam quality at the end of expansion in the steam turbine are key parameters for power generation in this low-temperature cycle. Additionally, they concluded that the HRSG represents the largest source of irreversibility, followed by the irreversibilities generated in the steam turbine body and the condenser [5].

Recent CCPP performance improvements primarily derive from gas turbine technological advancements, including advanced materials implementation, sequential combustion techniques, and elevated inlet exhaust gas temperatures (1300–1500 °C). Current research explores performance enhancement through alternative fuel compositions, particularly natural gas and hydrogen mixtures. Although these studies demonstrate thermal efficiency improvements, pure hydrogen integration introduces operational challenges, including a 9% reduction in exhaust gas mass flow. The HRSG configuration also significantly influences the system performance, with optimal results achieved through three-pressure-level systems [6,7].

The integration of renewable technologies with conventional fossil fuel systems represents a critical pathway for addressing escalating energy demands while mitigating environmental impacts. The strategic positioning of solar fields within HRSG systems demonstrates substantial efficiency potential, achieving 24.2% steam cycle power generation increases with 4 MW thermal input when integrated upstream of high-pressure superheaters. Additionally, solar field integration facilitates 7.97% fuel consumption reduction in gas turbines through compressor outlet air preheating prior to combustion chamber entry [8,9].

Power plant optimization methodologies increasingly incorporate exergy analysis for performance evaluation and enhancement. Exergy, defined as the maximum theoretical work obtainable from a material stream transitioning between initial and dead state conditions [10], provides critical insights into energy quality degradation throughout thermodynamic processes. This analytical framework enables the precise determination of component-specific and system-wide exergy efficiencies while identifying irreversibility sources and magnitudes [11,12]. Contemporary plant assessment methodologies integrate economic and thermodynamic analyses for comprehensive evaluation across diverse energy generation configurations.

Recent investigations have explored innovative power plant optimization approaches with promising results. Calise et al. conducted comparative thermoeconomic analyses of three-pressure-level combined cycle systems, contrasting conventional fossil fuel operation with hybrid solar field integration, demonstrating thermal efficiency improvements of 1% to 48.1% [13]. Mohammadi et al. investigated multifunctional hybrid systems incorporating gas turbines, organic Rankine cycles, and absorption refrigeration, achieving a 30 kW power generation, 8 kW cooling capacity, and 7.2 tons hot water production with a 67.6% thermal efficiency [14]. Ibrahim et al. identified primary energy loss mechanisms, with condensers exhibiting maximum energy losses, while combustion chambers demonstrated the highest exergy destruction rates [15]. Pacheco et al. conducted a thermodynamic study of a combined power and cooling generation system driven by geothermal energy. Their findings demonstrated that, using a 120 °C geothermal resource, the proposed system delivers a cooling capacity sufficient to preserve 3750 L of milk per day while simultaneously generating 12.53 kW of electrical power [16].

Advanced system integration studies have demonstrated significant performance improvements. Mohammadi et al. achieved a 40.75% exergy efficiency with annual product cost rates of 439 million dollars through the multi-objective optimization of organic Rankine cycle integration [17]. Similar configurations facilitated exhaust gas temperature reductions from 126 °C to 100 °C, generating an additional 12.4 MW power output [18]. The comprehensive exergy analysis by Gu et al. achieved a 52.35% exergy efficiency with 15.86 USD/h operational costs and 232.96 kg/MWh emissions [19].

Despite the extensive research on conventional CCPPs, limited attention has focused on hybrid configurations utilizing dual heat sources: gas turbine exhaust gases in HRSGs supplemented by dedicated steam generators (SGs). This configuration specifically addresses scenarios where the HRSG residual thermal energy proves insufficient for the total steam flow requirements. The present investigation offers a comprehensive thermodynamic characterization of the Valley of Mexico hybrid combined cycle (HCC) power plant across varying operational loads (100%, 75%, and 50%). The analysis commences with an energy performance evaluation under actual operating conditions, quantifying the critical parameters, including the power generation, heat supply distribution, thermal efficiency, pinch point temperature differentials, fuel and steam flow rates, and specific fuel consumption metrics. This study introduces and systematically evaluates the parameter β, defined as the heat supply ratio between SGs and HRSGs. This approach identifies the optimal heat distribution to maximize the system efficiency, revealing the operational conditions that minimize SG fuel consumption while optimizing the utilization of exhaust gas waste heat in HRSGs. The study culminates with a detailed exergy analysis under both actual operating conditions and varying β factor values, quantifying the internal irreversibility distributions and the overall system exergy efficiency. This methodological approach provides critical insights for the operational optimization of dual-heat-source power generation systems without necessitating significant capital investments.

2. Methodology

In this section, the methodology used for the thermodynamic analysis of the HCC power plant in the Valley of Mexico is presented. The study focuses on evaluating the plant's performance under real operating conditions, considering full (100%) and partial loads (75% and 50%). The methodology includes a detailed energy and exergy analysis, based on mass and energy balances, to determine the thermodynamic properties at each state of the cycle. Mathematical models are used to characterize the behavior of the GT and SC, considering the isentropic efficiencies of the equipment and reference environmental conditions. Additionally, the β factor, which represents the ratio between the heat flow

supplied by the SG and the HRSG, is introduced as a key parameter to determine an improvement in the power plant's performance.

2.1. Case Study

The thermodynamic analysis focuses on the Valley of Mexico thermoelectric power plant operating in hybrid mode, which integrates units 4, 5, 6, and 7, comprising a regenerative steam cycle with reheating and three gas turbines (GTs) coupled with their heat recovery steam generators (HRSGs). The analysis encompasses full-load (100%) and partial-load (75% and 50%) operations. The plant configuration varies according to the following operating conditions: at full load, it utilizes three GTs, three HRSGs, and one steam cycle (SC); at 75% load, two GTs, two HRSGs, and one SC; at 50% load, one GT, one HRSG, and one SC.

The HCC power plant of the Valley of Mexico, illustrated in Figure 1, consists of multiple integrated systems. The GT cycle incorporates a compressor, combustion chamber, and gas turbine, generating power for the electric generator (EG). Exhaust gases from the GT are directed to the HRSG for partial steam generation, while additional steam is produced by the steam generator (SG). The SC generates power through steam expansion in the high-pressure (HP), intermediate-pressure (IP), and low-pressure (LP) turbine sections.

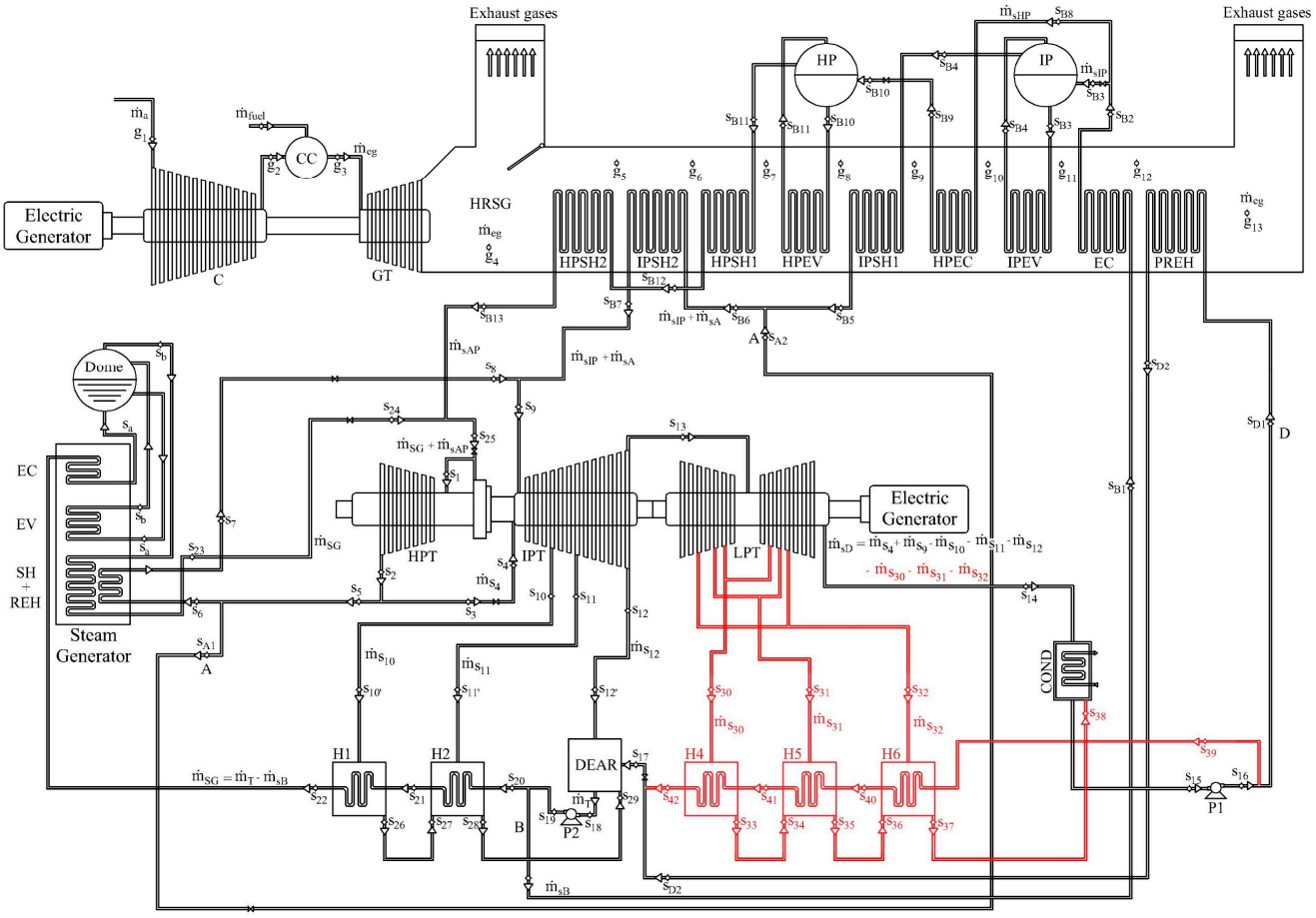


Figure 1. Hybrid combined cycle power plant of the Valley of Mexico.

The feedwater heating system comprises six closed feedwater heaters in a cascade configuration and an open feedwater heater, or deaerator (DEAR). Water exiting the DEAR undergoes pressurization above the HP and IP turbine inlet pressures before dividing into two streams for heating in the HRSG and SG. The HRSG stream undergoes preheating in the economizer (EC) before pressure regulation separates flows for the HP and IP sections.

The SG stream receives preheating through two IP closed heaters. After superheater (SH) exit, pressure regulation enables mixing with HPSH2 steam flow before HPT entry. The steam then expands to reheat pressure and receives additional heating in both the HRSG and SG reheaters (REH).

The reheated steam expands through the IPT, providing three extractions for heaters H2 and H3, and the DEAR. Under 100% and 75% loads, final expansion occurs in the LPT to condensation pressure. Condensate undergoes pressurization in pump P1 and preheating in the HRSG preheater (PREH) before DEAR entry.

At a 50% load operation, the system exhibits distinct characteristics. The IPT provides three steam extractions that supply low-pressure heaters H4, H5, and H6. After condensation, the pumped water flow divides into two streams for parallel preheating through the low-pressure heaters and the HRSG PREH. This configuration adaptation results from limited residual thermal energy availability in the single operational GT exhaust gases, which cannot provide sufficient preheating for the entire condenser exit steam flow.

2.2. Considerations

The thermodynamic analysis of the HCC power plant of the Valley of Mexico is conducted under the following considerations:

- The GT and SC with HRSG operate under steady-state conditions.
- The thermodynamic analysis is based on the actual operating conditions of the HCC power plant [20].
- The working fluids and air and combustion gases are considered ideal gases.
- The fuel used in the combustion chamber of the GT and in the SG is natural gas, with a composition of 88% CH_4, 10% C_2H_6, and 2% C_3H_8, having a lower heating value (LHV) of 49,514 kJ/kg_{fuel}.
- The thermodynamic properties of the steam cycle are determined using the CoolProp package in the Julia programming language.
- The equipment comprising the HCC power plant is considered adiabatic.
- The reference conditions for the pressure and temperature are P_0 = 0.78 bar and T_0 = 25 °C, respectively.

2.3. Energy Analysis

2.3.1. Energy Analysis of the Gas Turbine

Based on mass and energy balances applied to the gas turbine cycle, a set of equations is developed to determine the thermodynamic properties at each state. The pressure and temperature properties of the GT are determined based on the mathematical models presented in Table 1. These models are designed to calculate the pressures and temperatures of the GT based on the technological characteristics of the turbine, the properties of air and combustion gases, as well as the ambient conditions (see Appendix A).

Table 1. Thermodynamic states of the gas turbine cycle [21].

State	Pressure (Bar)	Temperature (°C)
g_1	P_{atm}	$T_{g_1} = T_{env}$
g_2	$P_{g_1}\ \pi_C$	$\frac{T_{g_2}}{T_{g_1}} = \left[1 + \frac{1}{\eta_{IC}}\left(\pi_C^{x_a} - 1\right)\right]$
g_3	$P_{g_2}(1 - \Delta P_{CC})$	T_{g_3}
g_4	$P_{g_1}(1 + \Delta P_{GT})$	$\frac{T_{g_4}}{T_{g_3}} = 1 - \eta_{IGT}\left[1 - \frac{(1+\Delta P_{GT})}{\pi_C(1-\Delta P_{CC})}\right]^{x_{eg}}$

The specific enthalpy at each thermodynamic state for the air and combustion gases in the *GT* cycle and *HRSG* is determined as follows:

$$h_{g_j} = c_{p_y}\left(\Delta T_{g_j-0}\right) y = a,\ eg \tag{1}$$

The specific entropy is calculated by

$$s_{g_j} = s_0 + c_{p_y}\ln\left(\frac{T_{g_j}}{T_0}\right) - R_y \ln\left(\frac{P_{g_j}}{P_0}\right) y = a,\ eg \tag{2}$$

The fuel-to-air ratio (*far*) of combustion is given by

$$far = \frac{1}{4.76\left(n+\frac{m}{4}\right)(1+\lambda)}\frac{MW_{C_nH_m}}{MW_a} \tag{3}$$

In the above expression, the excess air ratio, λ, is determined as follows:

$$\lambda = \frac{\left\{\begin{array}{c}\left[\Delta\overline{h}_f^o\right]_{C_nH_m} + \left(n+\frac{m}{4}\right)\left\{\left[\overline{h}_{T_{g2}} - \overline{h}_{T_{ref}}\right]_{O_2} + 3.76\left[\overline{h}_{T_{g2}} - \overline{h}_{T_{ref}}\right]_{N_2}\right\} - n\left[\Delta\overline{h}_f^o + \overline{h}_{T_{g3}} - \overline{h}_{T_{ref}}\right]_{CO_2} \\ +\frac{m}{2}\left[\Delta\overline{h}_f^o + \overline{h}_{T_{g3}} - \overline{h}_{T_{ref}}\right]_{H_2O} - 3.76\left(n+\frac{m}{4}\right)\left[\overline{h}_{T_{g3}} - \overline{h}_{T_{ref}}\right]_{N_2}\end{array}\right\}}{\left(n+\frac{m}{4}\right)\left\{\left[\overline{h}_{T_{g3}} - \overline{h}_{T_{g2}}\right]_{O_2} + 3.76\left[\overline{h}_{T_{g3}} - \overline{h}_{T_{g2}}\right]_{N_2}\right\}} \tag{4}$$

The air mass flow required by the *GT* to generate a given power is given by

$$\dot{m}_a = \frac{\dot{W}_{m,GT}}{c_{p_a}T_{g1}\left\{(1+far)\frac{c_{p_{eg}}}{c_{p_a}} y\eta_{IGT}\left[1 - \frac{(1+\Delta P_{GT})^{x_{eg}}}{[\pi_C(1-\Delta P_{CC})]^{x_{eg}}}\right] - \frac{1}{\eta_{IC}}\left(\pi_C^{x_a}-1\right)\right\}} \tag{5}$$

The heat flow supplied to the combustion chamber is

$$\dot{Q}_{sup,CC} = \dot{m}_a c_{p_a} T_{g1}\left[(1+far)\frac{c_{p_{eg}}}{c_{p_a}} y - 1 - \left(\frac{\pi_C^{x_a}-1}{\eta_{IC}}\right)\right] \tag{6}$$

The thermal efficiency of the *GT* cycle, defined as the ratio of the work output to the heat supplied to the combustion chamber, is expressed as

$$\eta_{th,GT} = \frac{\left\{(1+far)\frac{c_{p_{eg}}}{c_{p_a}} y\eta_{IGT}\left[1 - \frac{(1+\Delta P_{GT})^{x_{eg}}}{[\pi_C(1-\Delta P_{CC})]^{x_{eg}}}\right] - \frac{1}{\eta_{IC}}\left(\pi_C^{x_a}-1\right)\right\}}{(1+far)\frac{c_{p_{eg}}}{c_{p_a}} y - 1 - \frac{1}{\eta_{IC}}\left(\pi_C^{x_a}-1\right)} \tag{7}$$

2.3.2. Energy Analysis of the SC and HRSG

The steam cycle receives thermal energy from the following two sources: the exhaust gases in the *HRSG* and the supplementary heat from the steam generator (*SG*). The exhaust gases from the gas turbine provide heat to the *HRSG*, while additional heat comes from the natural gas combustion process in the steam generator. The total heat flow in the steam cycle is determined through

$$\dot{Q}_{sup,HRSG} = \dot{m}_{s_D}\Delta h_{s_{D2}-s_{D1}} + \left(\dot{m}_{s_{HP}} + \dot{m}_{s_{IP}}\right)\Delta h_{s_{B2}-s_{B1}} + \dot{m}_{s_{HP}}\Delta h_{s_{B13}-s_{B8}} + \dot{m}_{s_{IP}}\Delta h_{s_{B5}-s_{B3}} + \left(\dot{m}_{s_{IP}} + \dot{m}_{s_A}\right)\Delta h_{s_{B7}-s_{B6}} \tag{8}$$

$$\dot{Q}_{sup,SG} = \dot{m}_{s_{22}}\Delta h_{s_{23}-s_{22}} + \dot{m}_{s_6}\Delta h_{s_7-s_6} \tag{9}$$

The performance evaluation of the steam cycle utilizes key parameters. The thermal efficiency, representing the conversion effectiveness of heat input to mechanical power output, is expressed as

$$\eta_{th,SC} = \frac{\dot{W}_{m,SC}}{\dot{Q}_{sup,SG} + \dot{Q}_{sup,HRSG}} \tag{10}$$

An important operational parameter, the specific steam consumption (SSC), quantifies the steam mass required per kilowatt-hour of generated energy, as follows:

$$SSC = \frac{3600\ \dot{m}_{s_{total}}}{\dot{W}_{m,SC}} \tag{11}$$

The supplementary fuel requirement for the steam generator is determined through

$$\dot{m}_{fuel,SG} = \frac{\dot{Q}_{sup,SG}}{LHV} \tag{12}$$

Energy Balance in the HRSG

The HRSG analysis focuses on determining the intermediate temperatures throughout the heat exchanger sections. Based on the technical specifications of the Valley of Mexico thermoelectric power plant [20], the energy balances are established for each pressure section, as follows:

- High-pressure section

$$\text{HPSH2}: \ \dot{m}_{eg} c_{p_{eg}} \Delta T_{g_4 - g_5} = \dot{m}_{s_{HP}} \Delta h_{s_{B13} - s_{B12}} \tag{13}$$

$$\text{HPSH1}: \ \dot{m}_{eg} c_{p_{eg}} \Delta T_{g_6 - g_7} = \dot{m}_{s_{HP}} \Delta h_{s_{B12} - s_{B11}} \tag{14}$$

$$\text{HPEV}: \ \dot{m}_{eg} c_{p_{eg}} \Delta T_{g_7 - g_8} = \dot{m}_{s_{HP}} \Delta h_{s_{B11} - s_{B10}} \tag{15}$$

$$\text{HPEC}: \ \dot{m}_{eg} c_{p_{eg}} \Delta T_{g_9 - g_{10}} = \dot{m}_{s_{HP}} \Delta h_{s_{B9} - s_{B8}} \tag{16}$$

- Intermediate-pressure section

$$\text{IPSH2}: \ \dot{m}_{eg} c_{p_{eg}} \Delta T_{g_5 - g_6} = \left(\dot{m}_{s_{IP}} + \dot{m}_{s_A}\right) \Delta h_{s_{B7} - s_{B6}} \tag{17}$$

$$\text{IPSH1}: \ \dot{m}_{eg} c_{p_{eg}} \Delta T_{g_8 - g_9} = \dot{m}_{s_{IP}} \Delta h_{s_{B5} - s_{B4}} \tag{18}$$

$$\text{IPEV}: \ \dot{m}_{eg} c_{p_{eg}} \Delta T_{g_{11} - g_{10}} = \dot{m}_{s_{IP}} \Delta h_{s_{B4} - s_{B3}} \tag{19}$$

- Low-pressure section

$$\text{EC}: \ \dot{m}_{eg} c_{p_{eg}} \Delta T_{g_{11} - g_{12}} = \left(\dot{m}_{s_{HP}} + \dot{m}_{s_{IP}}\right) \Delta h_{s_{B2} - s_{B1}} \tag{20}$$

$$\text{PREH}: \ \dot{m}_{eg} c_{p_{eg}} \Delta T_{g_{12} - g_{13}} = \left(\dot{m}_{s_D}\right) \Delta h_{s_{D2} - s_{D1}} \tag{21}$$

The pinch point temperature differences, critical for the heat exchanger design and operation, are determined for both the high- and intermediate-pressure evaporators (HPEVs and IPEVs), as follows:

$$\Delta T_{PP_{HP}} = T_{g8} - T_{sat_{@P_{HP}}} \tag{22}$$

$$\Delta T_{PP_{IP}} = T_{g11} - T_{sat_{@P_{IP}}} \tag{23}$$

2.3.3. Energy Analysis for the HCC Power Plant of the Valley of Mexico

The total power output generated by the power plant is the sum of the power output from the *GT* cycle and the *SC*, as follows:

$$\dot{W}_{m,HCC} = \dot{W}_{m,SC} + \dot{W}_{m,GT} \tag{24}$$

The total heat flow supplied to the *HCC* is the sum of the heat flows supplied to the combustion chamber and the steam generator, as follows:

$$\dot{Q}_{sup,HCC} = \dot{Q}_{sup,SG} + \dot{Q}_{sup,CC} \tag{25}$$

Therefore, the total fuel flow supplied to the power plant is

$$\dot{m}_{fuel,HCC} = \dot{m}_{fuel,SG} + \dot{m}_{fuel,CC} \tag{26}$$

The thermal efficiency of the *HCC* is determined as a function of thermal efficiencies of *GT* and *SC* cycles, and the β factor, as follows:

$$\eta_{th,HCC} = \frac{\eta_{th,GT} + \eta_{th,SC} - \eta_{th,GT}\eta_{th,SC} + \beta(1-\eta_{th,GT})\eta_{th,SC}}{1 + \beta(1-\eta_{th,GT})} \tag{27}$$

where the β factor is the ratio of the heat flow supplied in the *SG* to the heat flow supplied in the *HRSG*, as follows:

$$\beta = \frac{\dot{Q}_{sup,SG}}{\dot{Q}_{sup,HRSG}} \tag{28}$$

Lower β values indicate greater utilization of exhaust gases in the *HRSG*, resulting in higher thermal efficiency for the system. Conversely, larger β values mean steam production shifts predominantly to the steam generator, reducing the overall thermal efficiency of the hybrid cycle as fuel consumption increases substantially.

Finally, the specific fuel consumption, which is the amount of fuel flow required to produce 1 kWh, is determined for the *GT*, *SC*, and *HCC* cycles as follows:

$$SFC_i = \frac{3600\ \dot{m}_{fuel,i}}{\dot{W}_{m,i}} \quad i = GT, SC \text{ and } HCCPP \tag{29}$$

2.4. Exergy Analysis

The exergy of a material stream is the maximum amount of work available that can be obtained by bringing the stream from its initial conditions to the dead state through reversible processes. In the absence of magnetic, electrical, and nuclear interactions, exergy is composed of its physical, chemical, kinetic, and potential components [10]. Neglecting the chemical, kinetic, and potential exergy, the exergy analysis conducted on the *HCC* power plant only considers the contribution of physical exergy, which is given by

$$\dot{E}_{ph,s_j} = \dot{m}_{s_k}\left(\Delta h_{s_j-0} - T_0 \Delta s_{s_j-0}\right) \tag{30}$$

Equation (30) is used to determine the exergy flow of the states in the *SC*. The physical exergy flow for the case of air and combustion gases as working fluids is given by

$$\dot{E}_{ph,y_j} = \dot{m}_y c_{p_y} T_0 \left[\left(\frac{T_{y_j}}{T_0} - 1\right) - \ln\frac{T_{y_j}}{T_0} - x_y \ln\frac{P_{y_j}}{P_0}\right] y = a,\ eg \tag{31}$$

The irreversibility flow in the components of the *HCC* power plant is determined through an exergy balance, expressed as

$$\dot{I}_i = \sum \dot{E}_{in,i} - \sum \dot{E}_{out,i} \tag{32}$$

Table 2 presents the exergy balances for the components of the power plant, where the total flow of irreversibilities for the plant is determined using Equation (32).

Table 2. Exergy balance of the components of the HCC power plant in the Valley of Mexico.

Component	$\sum \dot{E}_{in} - \sum \dot{E}_{out}$	Component	$\sum \dot{E}_{in} - \sum \dot{E}_{out}$
GT		SC	
C	$\left(\dot{E}_{g_1} - \dot{E}_{g_2}\right) + \dot{E}^{\dot{W}_C}$	HPT	$\left(\dot{E}_{s_1} - \dot{E}_{s_2}\right) - \dot{E}^{\dot{W}_{HPT}}$
CC	$\left(\dot{E}_{g2} - \dot{E}_{g3}\right) + \dot{E}_{fuel,CC}$	IPT	$\left(\dot{E}_{s_9} + \dot{E}_{s_4}\right) - \left(\dot{E}_{s_{10}} + \dot{E}_{s_{11}} + \dot{E}_{s_{12}} + \dot{E}_{s_{13}}\right) - \dot{E}^{\dot{W}_{IPT}}$
GT	$\left(\dot{E}_{g_3} - \dot{E}_{g4}\right) - \dot{E}^{\dot{W}_{GT}}$	LPT	$\dot{E}_{s_{13}} - \left(\dot{E}_{s_{30}} + \dot{E}_{s_{31}} + \dot{E}_{s_{32}} + \dot{E}_{s_{14}}\right) - \dot{E}^{\dot{W}_{LPT}}$
HRSG		SG	$\left(\dot{E}_{s_{22}} + \dot{E}_{s_6}\right) - \left(\dot{E}_{s_{23}} + \dot{E}_{s_7}\right) + \dot{E}_{fuel,SG}$
HPSH2	$\left(\dot{E}_{g_4} - \dot{E}_{g_5}\right) + \left(\dot{E}_{s_{B13}} - \dot{E}_{s_{B12}}\right)$	H1	$\left(\dot{E}_{s_{10'}} + \dot{E}_{s_{21}}\right) - \left(\dot{E}_{s_{22}} + \dot{E}_{s_{26}}\right)$
HPSH1	$\left(\dot{E}_{g_6} - \dot{E}_{g_7}\right) + \left(\dot{E}_{s_{B12}} - \dot{E}_{s_{B11}}\right)$	H2	$\left(\dot{E}_{s_{11'}} + \dot{E}_{s_{27}} + \dot{E}_{s_{20}}\right) - \left(\dot{E}_{s_{28}} + \dot{E}_{s_{21}}\right)$
HPEV	$\left(\dot{E}_{g_7} - \dot{E}_{g_8}\right) + \left(\dot{E}_{s_{B11}} - \dot{E}_{s_{B10}}\right)$	DEAR	$\dot{E}_{s_{12'}} + \dot{E}_{s_{17}} + \dot{E}_{s_{29}} - \dot{E}_{s_{18}}$
HPEC	$\left(\dot{E}_{g_9} - \dot{E}_{g_{10}}\right) + \left(\dot{E}_{s_{B9}} - \dot{E}_{s_{B8}}\right)$	H4	$\left(\dot{E}_{s_{30}} + \dot{E}_{s_{41}}\right) - \left(\dot{E}_{s_{33}} + \dot{E}_{s_{42}}\right)$
IPSH1	$\left(\dot{E}_{g_8} - \dot{E}_{g_9}\right) + \left(\dot{E}_{s_{B5}} - \dot{E}_{s_{B4}}\right)$	H5	$\left(\dot{E}_{s_{31}} + \dot{E}_{s_{34}} + \dot{E}_{s_{40}}\right) - \left(\dot{E}_{s_{35}} + \dot{E}_{s_{41}}\right)$
IPSH2	$\left(\dot{E}_{g_5} - \dot{E}_{g_6}\right) + \left(\dot{E}_{s_{B7}} - \dot{E}_{s_{B6}}\right)$	H6	$\left(\dot{E}_{s_{32}} + \dot{E}_{s_{39}} + \dot{E}_{s_{36}}\right) - \left(\dot{E}_{s_{37}} + \dot{E}_{s_{40}}\right)$
IPEV	$\left(\dot{E}_{g_{11}} - \dot{E}_{g_{10}}\right) + \left(\dot{E}_{s_{B4}} - \dot{E}_{s_{B3}}\right)$	COND	$\dot{E}_{s_{14}} + \dot{E}_{s_{38}} - \dot{E}_{s_{15}} - \dot{E}^{\dot{Q}_{COND}}$
EC	$\left(\dot{E}_{g_{11}} - \dot{E}_{g_{12}}\right) + \left(\dot{E}_{s_{B2}} - \dot{E}_{s_{B1}}\right)$	P1	$\dot{E}_{s_{15}} - \dot{E}_{s_{16}} + \dot{E}^{\dot{W}_{P1}}$
PREH	$\left(\dot{E}_{g_{12}} - \dot{E}_{g_{13}}\right) + \left(\dot{E}_{s_{D2}} - \dot{E}_{s_{D1}}\right)$	P2	$\dot{E}_{s_{18}} - \dot{E}_{s_{19}} + \dot{E}^{\dot{W}_{P2}}$

The exergy efficiency of the *GT* cycle is the power output generated by the system between the exergy flow of the fuel in the combustion chamber, as follows:

$$\eta_{exer,GT} = \frac{\dot{W}_{m,GT}}{\dot{E}_{fuel,CC}} \tag{33}$$

The exergy efficiency of the *SC* relates the power generated by the cycle to the sum of the exergy flow of the fuel supplied in the *SG* and the exergy flow of the exhaust gases in the *HRSG*.

$$\eta_{exer,SC} = \frac{\dot{W}_{m,SC}}{\dot{E}_{fuel,SG} + \dot{E}_{g_4 - g_{13}}} \tag{34}$$

Finally, the exergy flow of the *HCC* power plant is given by

$$\eta_{exer,HCC} = \frac{\dot{W}_{m,GT} + \dot{W}_{m,SC}}{\dot{E}_{fuel,CC} + \dot{E}_{fuel,SG}} \tag{35}$$

where the exergy flow of the fuel supplied in the combustion chamber and *SG* is

$$\dot{E}_{fuel,i} = \dot{m}_{fuel} LHV \left(1 - \frac{T_0}{T_{af}}\right) \quad i = CC \;\; y \;\; SG \tag{36}$$

Meanwhile, the exergy of the exhaust gases in the *HRSG* is expressed as follows:

$$\dot{E}_{eg,HRSG} = \dot{m}_{eg} c_{p_{eg}} T_0 \left[\left(\frac{T_{g4}}{T_0} - 1\right) - \ln \frac{T_{g4}}{T_0} - x_{eg} \ln \frac{P_{g1}(1 + \Delta P_{GT})}{P_0}\right] \tag{37}$$

Figure 2 displays the methodological flowchart for thermodynamic analysis of the *HCC* power plant in the Valley of Mexico. The process begins with atmospheric temperature and pressure initialization, followed by the gas turbine analysis. In this high-temperature system, thermodynamic properties are computed from the operational conditions, with performance parameters then derived through mathematical energy and exergy balance models. The exhaust gases (the flow rate and temperature) feed the steam cycle, where the pressures, temperatures, mass flows, and isentropic efficiencies of the turbines/pumps serve as inputs for the thermodynamic assessment. The heat recovery boiler is modeled ensuring positive pinch point temperature differences in both evaporators, enabling the energy/exergy performance quantification. The final stage integrates all parameters to evaluate the hybrid system's overall performance.

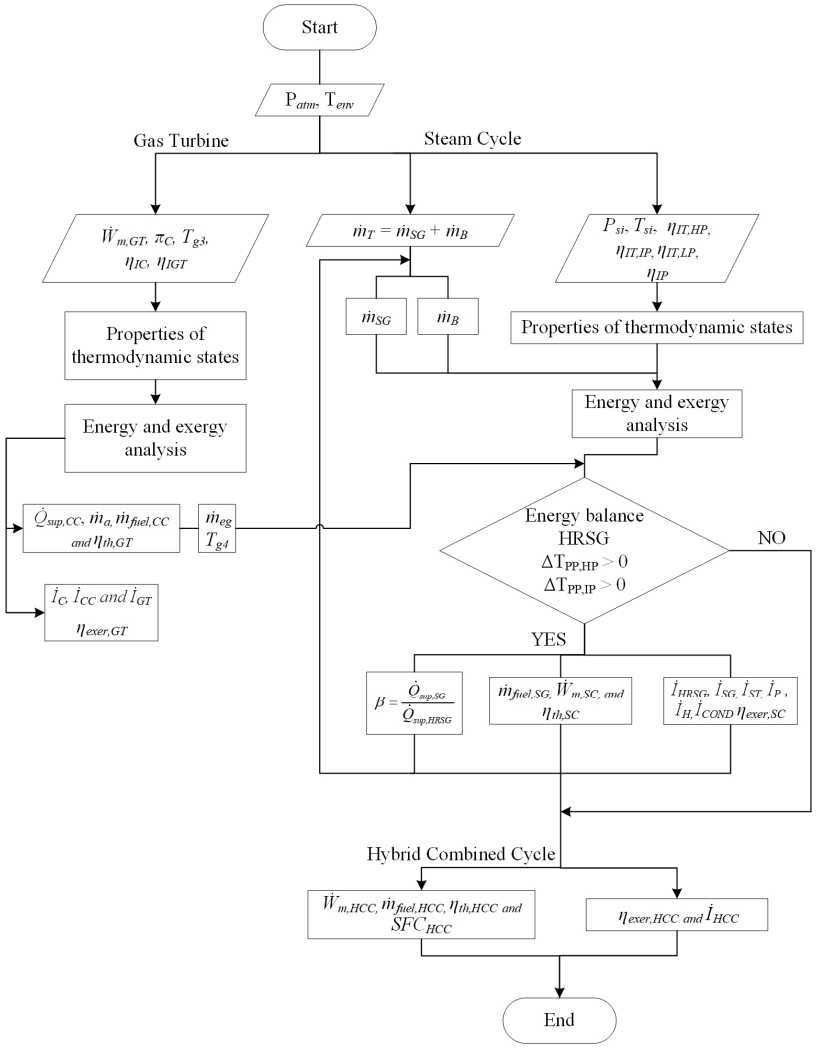


Figure 2. Flowchart of the proposed HCC power plant analysis methodology.

3. Results

In this section, the results of the thermodynamic analysis of the hybrid combined cycle power plant in the Valley of Mexico under actual operating conditions are initially presented. Key performance parameters, such as the power generation, thermal efficiency, specific fuel consumption, internal irreversibilities, and exergy efficiency, are discussed as a function of the load conditions. Subsequently, a thermodynamic analysis is conducted based on the variation in the β factor, aiming to evaluate the same performance parameters and determine the extent to which the power plant's performance can be improved.

3.1. Thermodynamic Analysis and Performance Characterization of the Valley of Mexico HCC Power Plant

3.1.1. Temperature–Entropy and Heat Transfer Analysis

The temperature–entropy diagrams and temperature profiles (Figure 3) illustrate the thermodynamic behavior of the HCC power plant under various operating conditions. The steam cycle presents distinctive characteristics at full and partial loads, with critical pinch point temperature differences, as shown in Table 3.

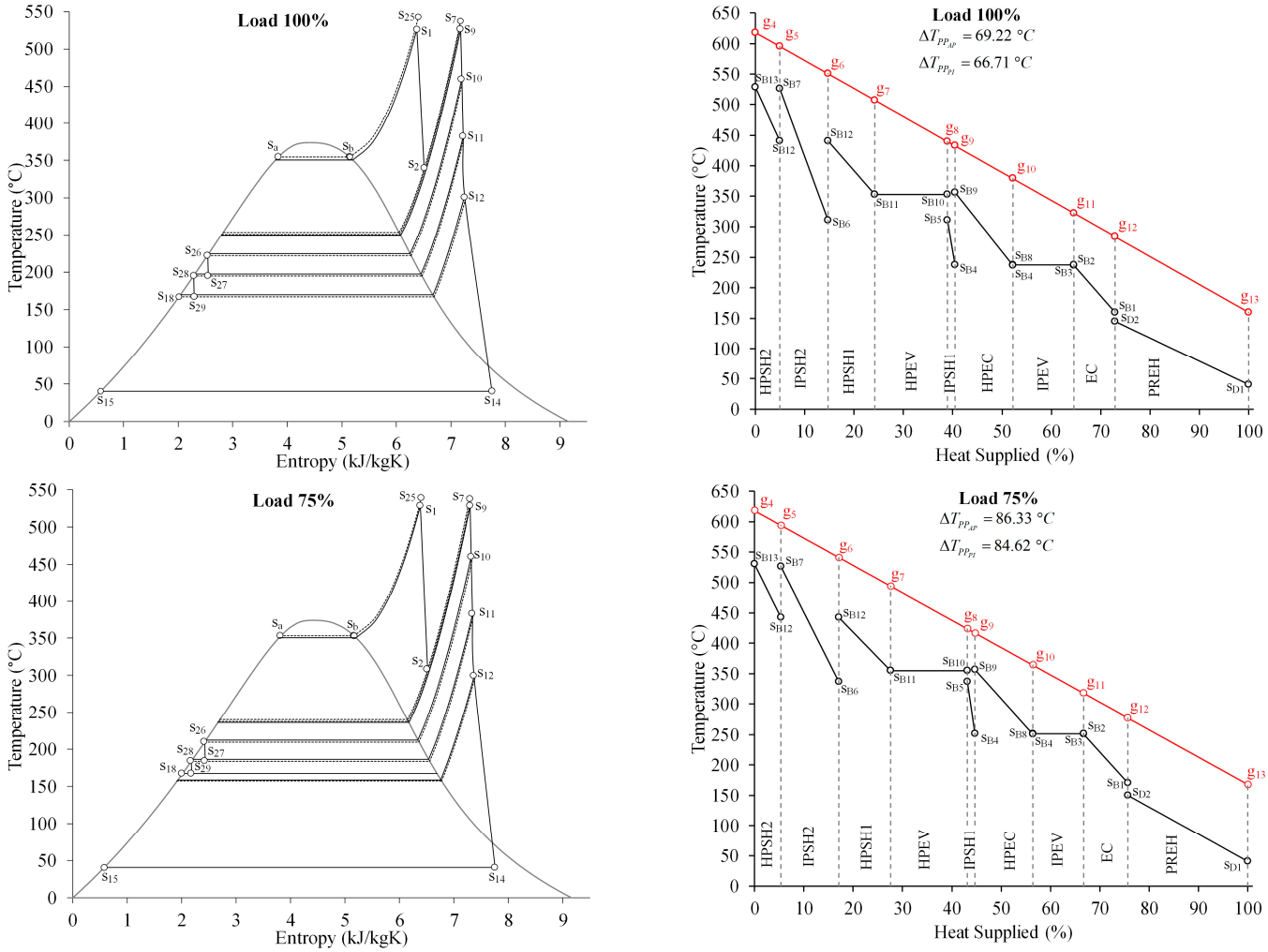


Figure 3. *Cont.*

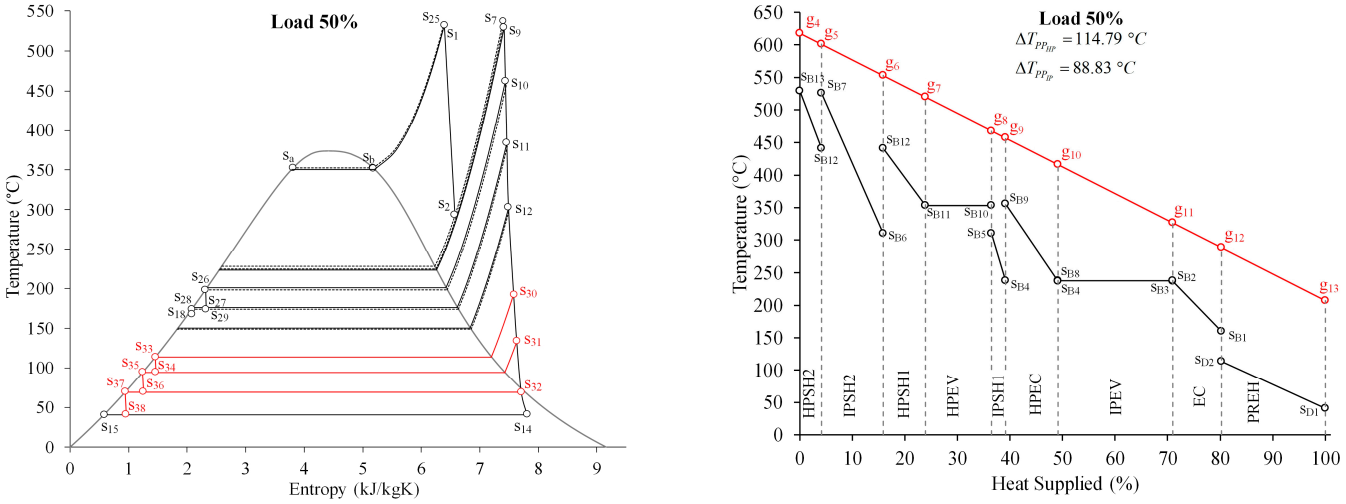


Figure 3. Temperature–entropy diagram and temperature profile of the CCH power plant in the Valley of Mexico at different loads.

Table 3. Critical temperature differences at various loads.

Load (%)	$\Delta T_{PP,HP}$ (°C)	$\Delta T_{PP,IP}$ (°C)
100	69.25	66.71
75	80.33	84.62
50	114.79	88.83

The temperature–entropy diagrams reveal that the steam generation in the SG (state s_{25}) occurs at pressure and temperature conditions marginally exceeding the HPT inlet requirements (state s1). After pressure reduction for mixing with the HPSH outlet flow, the steam undergoes reheating in the SG to temperatures above live steam conditions (state s_7). The reheating pressure remains below the HPT expansion endpoint pressure, indicating system pressure losses. The IPT operation features three steam extractions directed to heaters H2 and H3, and the deaerator, with extraction flows experiencing an average 5% pressure reduction.

At the 100% and 75% loads, steam expands in the turbine to condensation pressure conditions. The system configuration adapts at a 50% load, incorporating three steam extractions to heaters C4, C5, and C6. Temperature profiles demonstrate that the high-pressure section heat exchangers achieve maximum heat transfer percentages, with remaining thermal energy distributed across the intermediate-pressure sections, PREH, and EC.

The PREH and EC, responsible for preheating the high- and intermediate-pressure steam flows, show decreasing heat transfer percentages with load reduction, reaching minimum values at a 50% load (20% in the PREH). This reduction results from combined preheating effects in the HRSG and IPT extractions. Conversely, the HPSH2 + IPSH1 + HPSH1 assembly exhibits an increased heat transfer percentage as the load decreases, corresponding to the enhanced steam flow ($\dot{m}_A$) through IPSH2.

3.1.2. Exergy Analysis and Performance Characteristics

Figure 4 presents exergy–enthalpy diagrams and exergy profiles across operating loads. Maximum exergy occurs at live steam pressure and temperature conditions, while peak energy appears at reheating conditions. The HPT expansion and first two IPT expansions contribute approximately 45% of the useful work output, with the remaining work generated in the final IPT expansion and LPT (single expansion at the 100% and 75% loads, and four expansions at a 50% load).

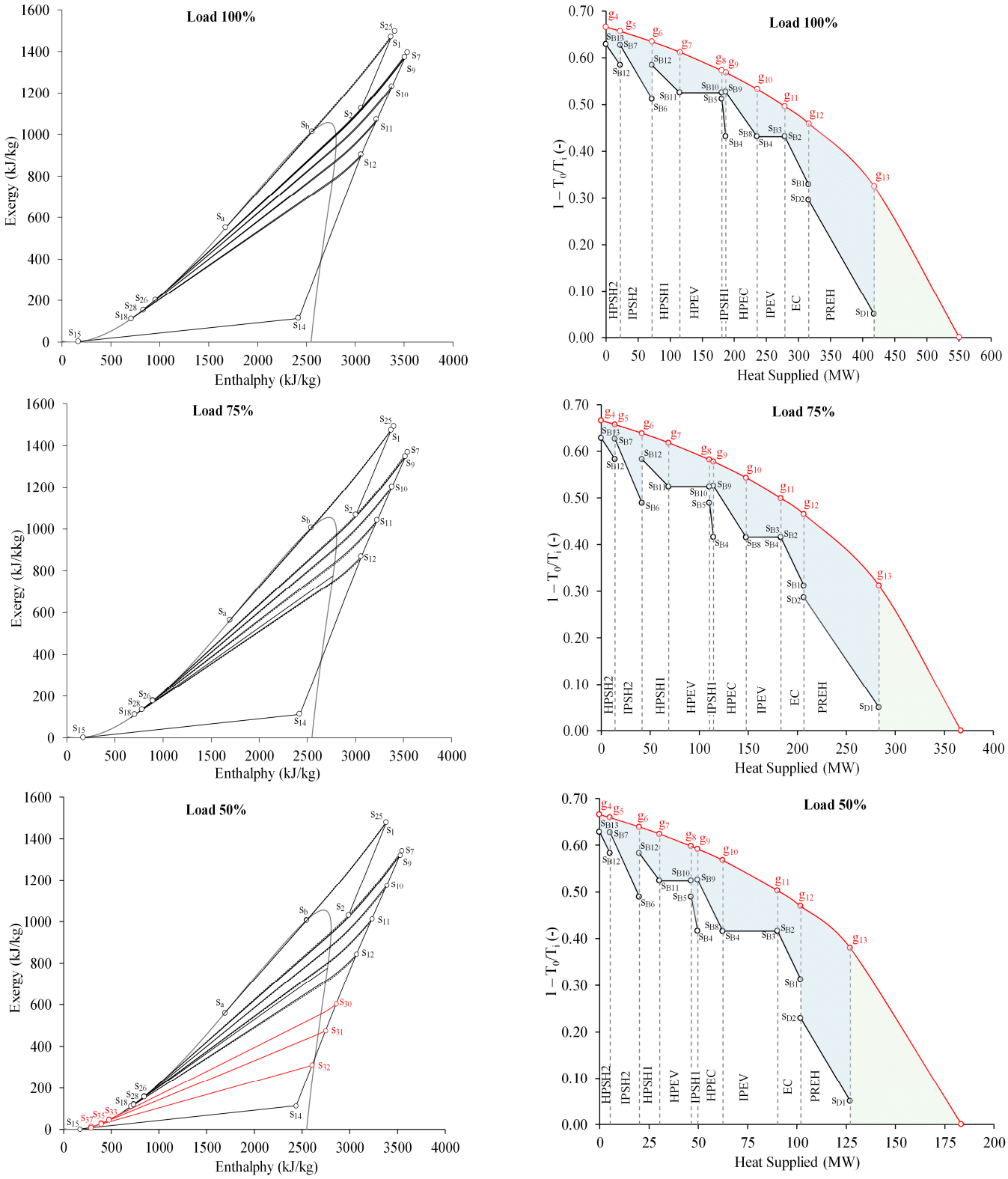


Figure 4. Exergy–enthalpy diagram and exergy profile of the HCC power plant in the Valley of Mexico at different loads.

Steam exiting the LPT maintains significant energy content but minimal availability, reaching 1.4 kJ/kg exergy at the condenser outlet. The feedwater heating train increases the energy availability by 200 kJ/kg before SG entry. The exergy profiles demonstrate heat

transfer effectiveness in the HRSG components, with internal irreversibilities represented by the area between the exhaust gas and steam streams.

The PREH exhibits maximum irreversibility due to highest heat supply and stream separation, though these losses decrease with the load reduction from 100% to 50%. The high- and intermediate-pressure superheating sections generate minimal irreversibilities. The HPEV and IPEV maintain relatively constant heat supply flows across loads, with irreversibility primarily influenced by PP temperature differences, which is particularly pronounced in the IPEV. External irreversibility, represented by exhaust gases (state g_{13}) exiting through the stack, shows slight increases at reduced loads due to the elevated HRSG outlet temperatures. The behavior of the internal irreversibilities generated in both the superheaters and evaporators aligns with the findings reported in the combined cycle power plant literature [22].

This thermodynamic characterization enables performance optimization through β factor adjustment while maintaining positive PP temperature differences to prevent temperature crossovers between the steam and exhaust gas streams.

3.2. Performance Parametric Analysis of the Valley of Mexico HCC Power Plant Through β Factor Variation

3.2.1. Energy Analysis Through β Factor Variation

The energy analysis of the Valley of Mexico HCC power plant reveals significant performance relationships when varying the β factor under different load conditions. Figure 5 illustrates the thermal efficiency, power output, and fuel flow behavior as functions of the β factor variation. Across all operating scenarios, a consistent pattern emerges: lower β values correspond to increased power generation and thermal efficiency while reducing the required fuel flow. Conversely, higher β values lead to decreased power generation and thermal efficiency, accompanied by increased fuel consumption, primarily because steam generation shifts predominantly to the steam generator. These findings demonstrate a direct correlation between the β parameter and plant operation mode: lower β values drive the system toward conventional combined cycle behavior, while higher values promote the operation characteristics typical of traditional thermal power plants.

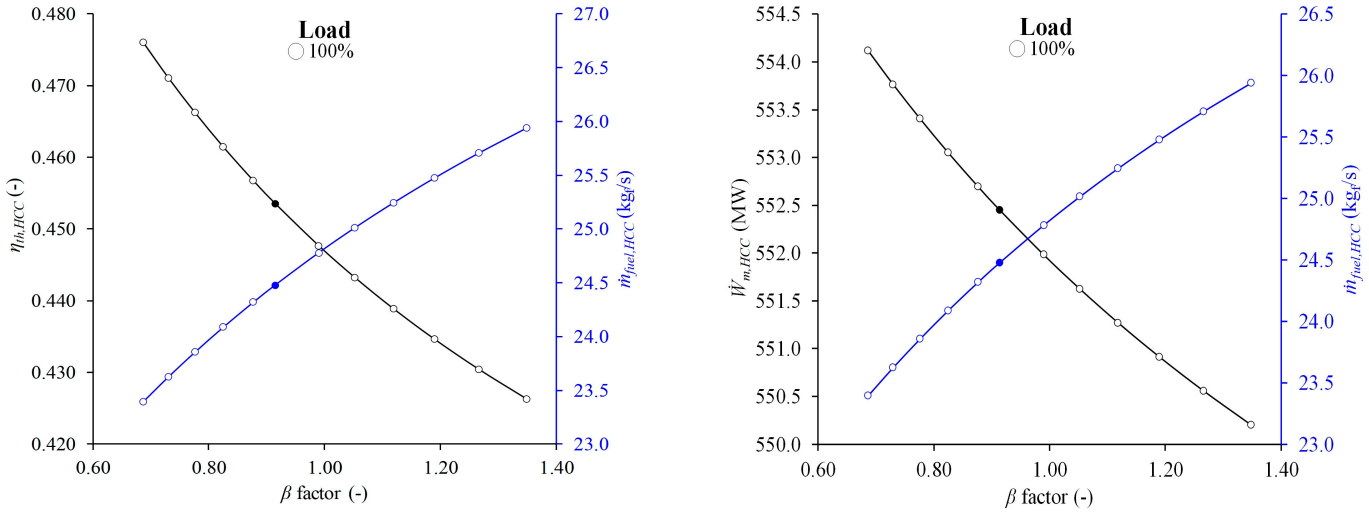


Figure 5. *Cont.*

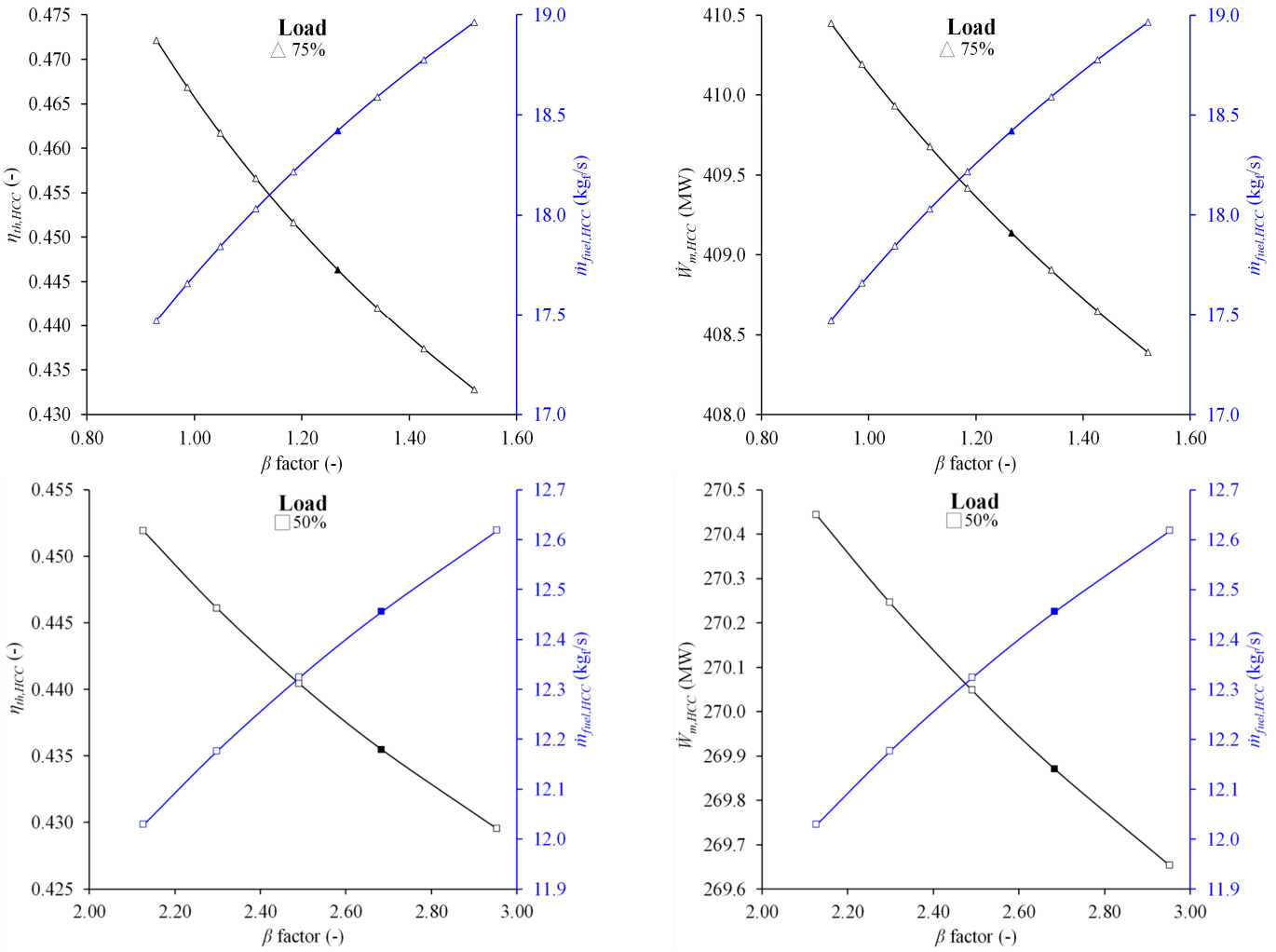


Figure 5. Thermal efficiency and power generation of the HCC power plant in the Valley of Mexico as a function of the β factor at different loads.

At a 100% load, the plant operates with a β factor of 0.91, generating 552.45 MW at a 45.36% thermal efficiency while consuming 24.48 kg_{fuel}/s. However, operational improvements become evident at reduced β values. At β = 0.69, the power generation increases by 1.67 MW, the thermal efficiency improves by 2.25 percentage points, and fuel consumption decreases by 1.08 kg_{fuel}/s compared to the actual operating conditions. This efficiency improvement occurs because lower β values reduce steam generator production and intermediate-pressure turbine extraction flow for the heating train, while increasing the HRSG steam generation.

Under 75% load conditions, with only two gas turbines operating, the steam cycle functions with a β factor of 1.27, indicating predominant steam generator reliance. The analysis shows potential operation at β = 0.93, which would increase the power generation by 1.31 MW, reduce the fuel consumption by 0.95 kg_{fuel}/s, and increase the thermal efficiency to 47.22%.

At the minimum load (50%), with only one operational gas turbine, the system operates at a β factor of 2.13, demonstrating substantial steam generator dependence. Consequently, performance improvements are more modest than at higher loads, with potential power generation increases of just 0.57 MW, thermal efficiency improvements of 1.64 percentage points, and fuel flow reductions of 0.42 kg_{fuel}/s.

Figure 6 illustrates the distribution of power generation across steam turbine sections as a function of the β factor. The intermediate- and low-pressure sections maintain relatively

consistent output regardless of the β variation. However, power contribution sources undergo substantial shifts: at full load, HRSG-generated steam provides most of the power, while, at partial loads (75% and 50%), the steam generator flow becomes the predominant source of power production. The high-pressure turbine section demonstrates pronounced sensitivity to β factor variations, with the steam generator flow contributing significantly to the power generation. This section exhibits greater responsiveness to steam source changes than other turbine stages.

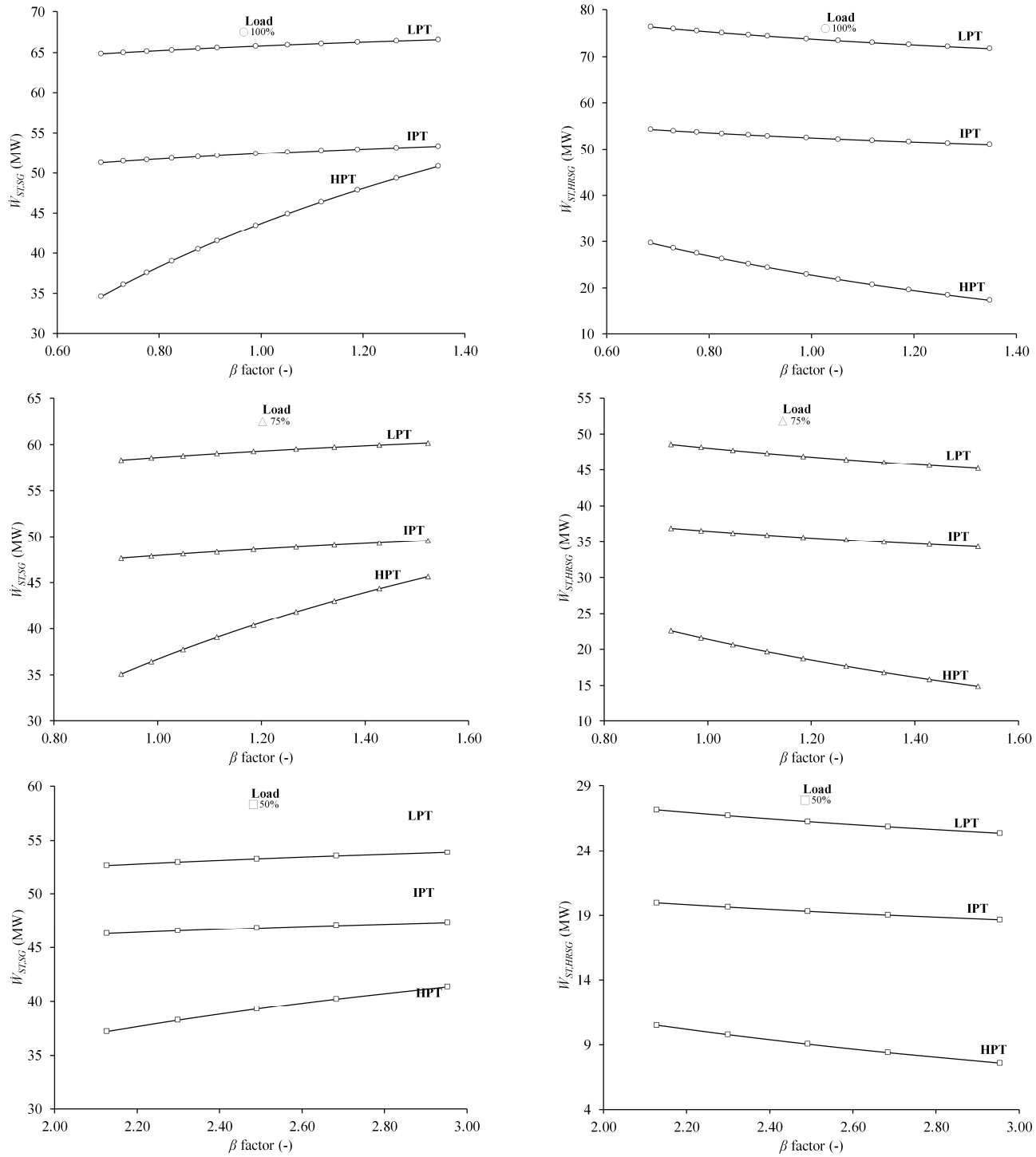


Figure 6. Power generated by sections of the steam turbine as a function of the β factor at different loads.

Specific fuel consumption (SFC) trends, shown in Figure 7, confirm the optimization opportunities at lower β values. Minimum SFC values of 0.1519, 0.1532, and 0.1601 kg_{fuel}/kWh occur at β values of 0.69, 0.93, and 2.13 for the 100%, 75%, and 50% loads, respectively. Under actual operating conditions, the SFC increases to 0.1595 kg_{fuel}/kWh at full load and rises further to 0.1620 and 0.1661 kg_{fuel}/kWh at 75% and 50% loads.

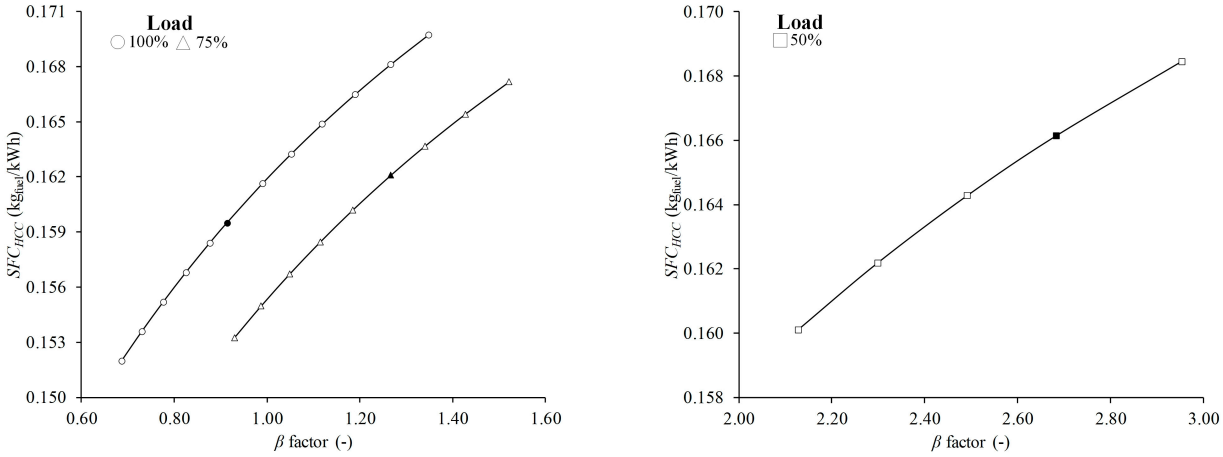


Figure 7. SFC of the HCC power plant in the Valley of Mexico as a function of the β factor at different loads.

3.2.2. Exergy Analysis

Figure 8 presents the Grassmann diagram of the GT cycle, with exergy flow quantities corresponding to three gas turbines collectively. The fuel exergy flow constitutes the sole external resource entering the system through the combustion chamber, alongside air exergy flow from the compressor outlet. The combustion chamber generates internal irreversibility due to the heat supply process, while producing high-quality exergy flow ($\dot{E}_{g3}$) that drives both turbine power production and compressor operation. Exhaust gas exergy ($\dot{E}_{g4}$) transfers to the HRSG, where a portion ($\Delta\dot{E}_{ge} = \dot{E}_{g4} - \dot{E}_{g13}$) increases the steam exergy in high- and intermediate-pressure sections while preheating the condenser outlet water.

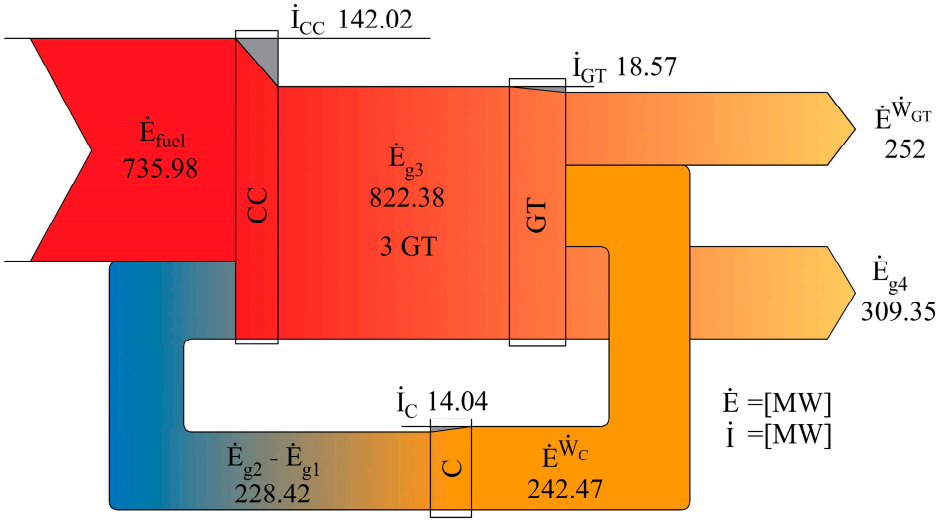


Figure 8. Grassmann diagram of the GT cycle of the HCC power plant in the Valley of Mexico.

Figure 9 presents the Grassmann diagram of the steam cycle. This diagram shows how two external resource streams, the exergy flow from exhaust gases utilized in the

HRSG ($\Delta\dot{E}_{g4-g13}$) and the fuel exergy supplied to the steam generator, contribute to power generation across all turbine sections. The exergy flow entering the high-pressure turbine ($\dot{E}_{s1}$) originates from the following three sources: the steam generator, the feedwater heating train ($\dot{E}_{s21}$), and the HRSG high-pressure section. During expansion through the HPT, this exergy produces power to fuel the cycle pumping system and generates irreversibilities inherent to the expansion process. After high-pressure expansion, the remaining exergy combines with additional flows from the steam generator reheater and the HRSG intermediate-pressure section. This combined flow ($\dot{E}_{s9}$) enters the intermediate-pressure turbine, where it generates power, creates some irreversibilities, and diverts a portion of its exergy to recirculate through the feedwater heating train. The exergy remaining after these processes serves as the input for the low-pressure turbine, where it divides between useful power output and the residual exergy flow discharged to the condenser.

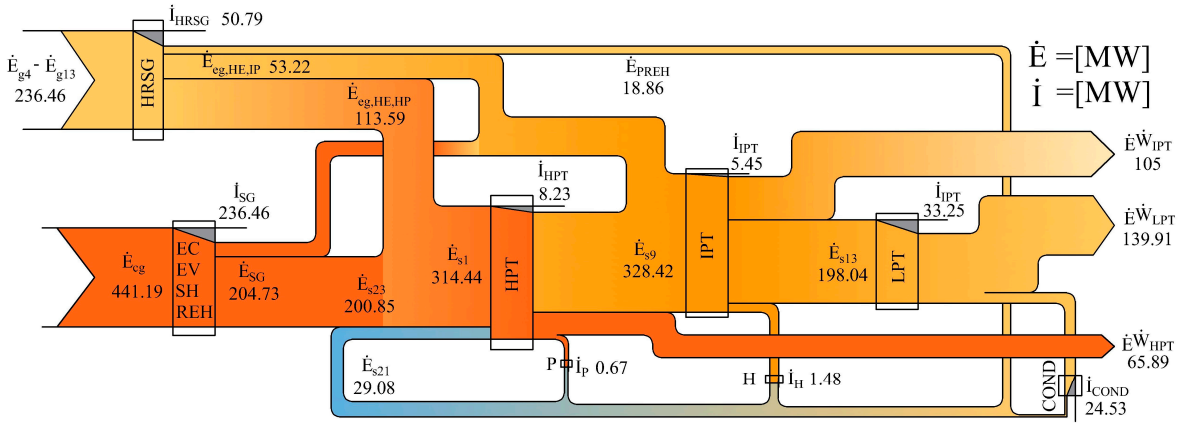


Figure 9. Grassmann diagram of the SC and HRSG of the HCC power plant in the Valley of Mexico.

Figure 10 illustrates the relationship between the exergy efficiency, total irreversibility flow, and the β factor across different HCC power plant loads. Under actual operating conditions, decreasing the β factor leads to increased exergy efficiency and reduced irreversibility flow. These improvements become most pronounced at the 100% and 75% loads, where the operational conditions permit greater steam generation through the HRSG. This enhanced HRSG utilization reduces the exergy flow of fuel supplied to the SG, thereby decreasing irreversibilities primarily generated in this equipment.

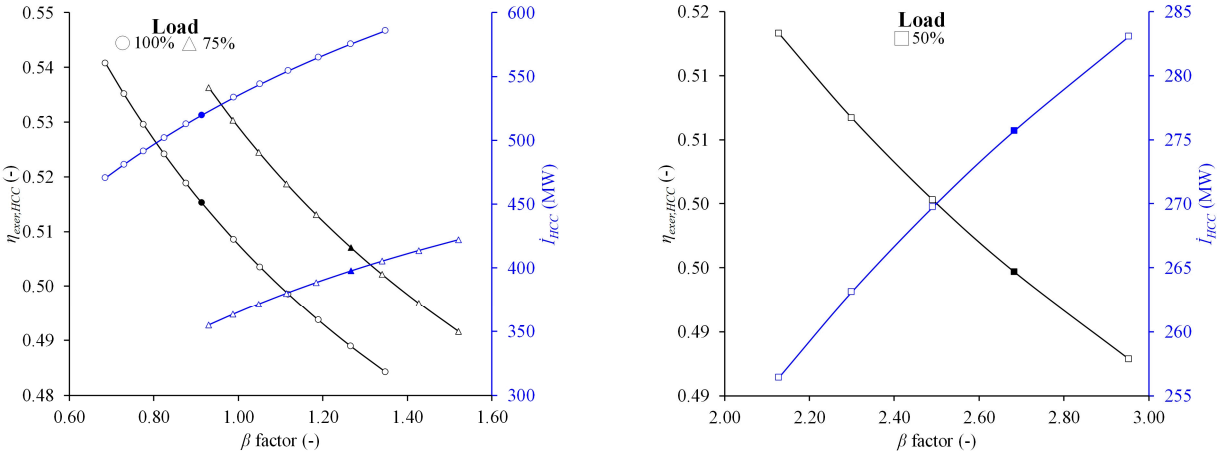


Figure 10. Exergy efficiency and irreversibility flow of the HCC power plant in the Valley of Mexico as a function of the β factor at different loads.

The total irreversibility flow reduction reaches 49 MW at full capacity operation and 42 MW at a 75% load operation, corresponding to the lowest β factors of 0.69 and 0.93, respectively. For these same β values, the exergy efficiency ranges between 0.535 and 0.540. Under minimum-load conditions (50%), operational constraints limit steam generation through the HRSG due to reduced exhaust gas availability and, consequently, a decrease in the exergy efficiency. This results in greater reliance on the steam generator (SG) to maintain the required steam flow, which increases the fuel supply and, therefore, irreversibilities in this equipment. Although HRSG utilization is lower compared to the 100% and 75% loads, the analysis remains relevant to understanding the system behavior under partial-load conditions. In this case, the maximum achievable exergy efficiency remains below 0.52, with potential reductions in the irreversibility flow of approximately 20 MW compared to the actual operating conditions. The exergy efficiency and total irreversibility flow values obtained for the HCC align with those reported in the literature, where conventional systems achieve exergy efficiencies of 57.63%. This agreement suggests that a further reduction in the β factor beyond current values would drive the system closer to the characteristic performance of a conventional combined cycle [22].

Figure 11 presents the exergy flow, irreversibilities, and power generated by the power plant under actual operating conditions. The fuel exergy flow distributes primarily into useful product, corresponding to the power output, while the remaining portion manifests as internal irreversibilities generated by the equipment and external irreversibilities associated with the exhaust gases discharged from the HRSG. The analysis of all three operating conditions reveals that most of the exergy destruction occurs during heat supply processes in the combustion chamber and steam generator, as well as through the exhaust gas exergy flow, $\dot{E}_{g13}$. The irreversibilities from expansion processes in both the gas turbine and the three steam turbine sections remain significantly lower. Equipment, including the compressor, condenser, heat exchangers in the HRSG, and feedwater heating train contribute the smallest amounts of irreversibilities to the overall power system.

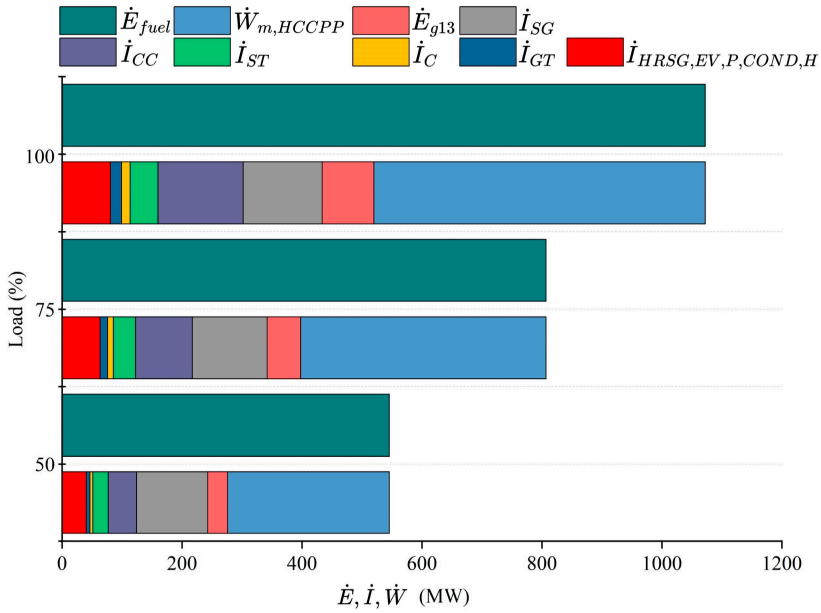


Figure 11. Exergy flow, irreversibility, and power output of the HCC power plant in the Valley of Mexico at different loads.

4. Conclusions

This study presents a comprehensive thermodynamic analysis of the operational hybrid combined cycle power plant in the Valley of Mexico under actual operating conditions.

The investigation introduces the β factor as a critical parameter for system optimization, revealing significant performance enhancement opportunities through strategic heat flow management.

The analysis demonstrates that β factor reduction from current operating values (0.91 at 100% load, 1.27 at 75% load, and 2.13 at 50% load) offers substantial benefits. At full-load operation, reducing the β value to 0.69 increases the power generation by 1.67 MW, improves the thermal efficiency by 2.25 percentage points, and reduces the fuel consumption by 1.08 kg_{fuel}/s. Similarly, at a 75% load, optimizing the β value to 0.93 yields power gains of 1.31 MW and fuel savings of 0.95 kg_{fuel}/s, while elevating the thermal efficiency to 47.22%.

The exergy analysis provides deeper insights into these improvements, revealing that optimized β values reduce the irreversibility generation by up to 49 MW at full capacity and 42 MW at a 75% load, with corresponding exergy efficiencies reaching 53.5–54.0%. These gains result primarily from the enhanced exhaust gas utilization in the HRSG, which substantially reduces the entropy generation in the heat transfer processes.

Detailed component analysis identifies the combustion chamber and steam generator as the primary sources of exergy destruction, accounting for over 65% of system irreversibilities. This finding underscores the thermodynamic advantage of shifting the heat supply from direct combustion toward waste heat recovery whenever operationally feasible.

The varying performance responses across load conditions reveal important operational considerations. The full-load and 75% load conditions demonstrate greater optimization potential through β factor adjustment, while 50% load operations show more constrained improvement opportunities, suggesting that different operational strategies may be optimal depending on grid demand conditions.

These findings have significant practical implications for both existing plant operations and future design considerations. For operational plants, implementing control strategies that minimize β values while maintaining system stability could yield immediate efficiency gains without capital-intensive modifications. For future designs, these results suggest potential benefits from the increased HRSG capacity relative to conventional configurations, particularly for installations designed for predominantly high-load operation.

Beyond efficiency improvements, the identified fuel consumption reductions translate to proportional decreases in greenhouse gas emissions, aligning with broader sustainability objectives. Based on standard natural gas emission factors, the potential fuel savings at full-load operation, as well as at partial loads of 75% and 50%, will reduce CO_2 emissions by approximately 82,024.96, 36,852.19, and 32,852.19 tons annually, respectively.

Further research should explore dynamic β factor optimization strategies, investigate potential equipment modifications to expand the operational range of lower β values, and evaluate economic payback periods for implementing such optimizations across different power generation portfolios.

Author Contributions: Conceptualization, R.L.-L., M.S.-P. and L.E.M.-C.; methodology, R.L.-L. and L.E.M.-C.; software, L.E.M.-C.; validation, R.L.-L., H.D.L.-M. and L.E.M.-C.; formal analysis, R.L.-L., M.S.-P. and L.E.M.-C.; investigation, M.S.-C., M.S.-P. and L.E.M.-C.; resources, R.L.-L., M.S.-P., A.T.-A., H.D.L.-M. and M.S.-C.; data curation, L.E.M.-C.; writing—original draft preparation, R.L.-L., L.E.M.-C. and M.S.-P.; writing—review and editing, M.S.-C., H.D.L.-M., R.L.-L. and L.E.M.-C.; visualization, L.E.M.-C. and A.T.-A.; supervision, M.S.-P. and R.L.-L.; project administration, H.D.L.-M. and M.S.-C. All authors have read and agreed to the published version of the manuscript.

Funding: This research received no external funding.

Data Availability Statement: The original contributions presented in the study are included in the article, further inquiries can be directed to the corresponding authors.

Conflicts of Interest: The authors declare no conflict of interest.

Nomenclature

Abbreviations

C	compressor
CC	combustion chamber
CCPP	combined cycle power plant
COND	condenser
DEAR	deaerator
EC	economizer
EG	electrical generator
EV	evaporator
GT	gas turbine
H	heater
HCC	hybrid combined cycle
HP	high pressure
HRSG	heat recovery steam generator
IP	intermediate pressure
LP	low pressure
P	pump
PREH	preheater
REH	reheater
SC	steam sycle
SG	steam generator
SH	superheater
T	turbine

Subscripts

0	dead state
a	air
af	adiabatic flame
atm	atmospheric
env	environmental
exer	exergetic
fuel	fuel
eg	exhaust gases
$g_1,\ldots,g_{13}$	thermodynamic states of the gas turbine cycle and the HRSG
IC	compressor isoentropic efficiency
IGT	gas turbine isoentropic efficiency
in	inlet
m	output
out	outlet
p	constant pressure
ph	physical
PP	pinch point
ref	reference
$s_1,\ldots,s_{42}$	thermodynamic states of the steam cycle
$s_{D1},\ldots,s_{D2}$	
$s_{B1},\ldots,s_{B13}$	
$s_{A1},\ldots,s_{A2}$	
sup	supplied
th	thermal

Symbols

c	specific heat	(kJ/kg K)
far	air–fuel ratio	(kg_a/kg_{fuel})
h	enthalpy per unit mass	(kJ/kg)
$\dot{I}$	flow of irreversibilities	(kW)
LHV	low heating value	(kJ/kg_{fuel})
MW	molecular weight	(kg/kmol)
$\dot{m}$	mass flow	(kg/s)
P	pressure	(bar)
$\dot{Q}$	heat flow	(kW)
R	ideal gas constant	(kJ/kg K)
s	entropy per unit mass	(kJ/kg K)
SFC	specific fuel consumption	(kg_{fuel}/kWh)
q	heat supplied per unit mass	(kJ/kg)
T	temperature	(°C)
$\dot{W}$	power	(MW)
x	relation between adiabatic index ($\gamma - 1/\gamma$)	(-)
y	relation between temperatures (T_{g3}/T_{g1})	(-)

Greek letters

$\dot{E}$	exergy flow	(kW)
γ	adiabatic index	(-)
Δ	increment	(-)
η	efficiency	(-)
λ	excess air	(-)
π	pressure ratio	(-)

Appendix A

Table A1 presents the operating conditions of the power plant at full-load and partial-load conditions. Initially, the operating conditions of the gas turbine are detailed. Likewise, for the steam cycle, the pressure and temperature conditions of the main states are included, which are necessary to determine the thermodynamic properties at all stages of the cycle. Additionally, the main steam flows are specified, as well as the isentropic efficiencies of the steam turbine sections and the pumps.

Table A1. Actual operating conditions of the HCC power plant in the Valley of Mexico at different loads.

GT			
π_C (-)	11.4	η_{IGT} (-)	0.9
ΔP_{GT} (-)	0.04	T_{g1} (°C)	25
ΔP_{CC} (-)	0.04	T_{g3} (°C)	1150
η_{IC} (-)	0.88	$\dot{W}_{m,GT}$ (MW)	84
SC			
Pressure (bar)			
		Load (%)	
State	100	75	50
s_1		166.5	
s_2	42.5	33.4	26.9
s_8	40.54	32	25.5
s_{10}	25.37	20	15.8
$s_{10'}$	24.10	18.99	15

Table A1. *Cont.*

s_{11}	14.72	11.6		9.13
$s_{11'}$	13.99	10.97		8.67
s_{12}	7.79		6.02	
$s_{12'}$	7.40		5.72	
s_{30}	-	-		1.62
s_{31}	-	-		0.82
s_{32}	-	-		0.3
s_{19}		198		
s_{23}	174.1	172		170
s_{14}		0.078		
s_{D1}		15		
s_{B3}	40.54	32		25.5
Temperature (°C)				
Load (%)				
State	100	75		50
s_1	526.5	529		532
s_9	526.7	528		529.7
s_{23}	537.8	538		537.8
s_7	537.8	538		537.8
s_{D2}		148.1		
s_{B7}	516		511.5	
s_{B13}		514		
Steam mass flow (kg_s/s) and isoentropic efficiency of turbine and pump (-)				
$\dot{m}_s$	100%	75%		50%
T	239.05	188.38		148.95
B	104.30	69.35		34.57
SG	134.75	119.04		114.38
A	92.03	57.55		30.73
HP	79.27	50.22		23.91
IP	25.03	19.13		10.67
s_{10}	6.71	5.46		5.25
s_{11}	5.69	4.78		4.60
s_{12}	6.31	3.22		9.52
s_{30}	-	-		1.78
s_{31}	-	-		2.08
s_{32}	-	-		2.19
s_{39}	-	-		47.56
$\eta_{IT,HP}$ (-)	0.79	0.84		0.80
$\eta_{IT,IP}$ (-)	0.90	0.91		0.91
$\eta_{ST,LP}$ (-)	0.80	0.84		0.84
η_{IP} (-)		0.85		

References

1. Méndez-Cruz, L.E.; Salazar-Pereyra, M.; Bonilla-Blancas, A.E.; Lugo-Leyte, R. Análisis Termodinámico de las Turbinas de Vapor para los Ciclos Ultracríticos, Supercríticos, Subcríticos y Geotérmicos. *Inf. Tecnológica* **2019**, *30*, 237–248. [CrossRef]
2. Lugo, R.; Salazar, M.; Zamora, J.M.; Torres, A.; Toledo, M. Análisis exergético de una central termoeléctrica. *Científica* **2009**, *13*, 17–25.
3. Shireef, L.T.; Ibrahim, T.K. Influence of operating parameters on the performance of combined cycle based on exergy analysis. *Case Stud. Therm. Eng.* **2022**, *40*, 102506. [CrossRef]
4. Kotowicz, J.; Brzęczek, M. Analysis of increasing efficiency of modern combined cycle power plant: A case study. *Energy* **2018**, *153*, 90–99. [CrossRef]
5. Aliyu, M.; AlQudaihi, A.B.; Said, S.A.M.; Habib, M.A. Energy, exergy and parametric analysis of a combined cycle power plant. *Therm. Sci. Eng. Prog.* **2020**, *15*, 100450. [CrossRef]

6. Jamróz, M.; Piwowarski, M.; Ziemiański, P.; Pawlak, G. Technical and economic analysis of the supercritical combined gas-steam cycle. *Energies* **2021**, *14*, 2985. [CrossRef]
7. Mustafa, L.; Ślefarski, R.; Jankowski, R. Thermodynamic Analysis of Gas Turbine Systems Fueled by a CH_4/H_2 Mixture. *Sustainability* **2024**, *16*, 531. [CrossRef]
8. Abdelhalim, A.M.; Meana-Fernández, A.; Suarez-Ramon, I. Integration of Thermal Solar Power in an Existing Combined Cycle for a Reduction in Carbon Emissions and the Maximization of Cycle Efficiency. *Processes* **2024**, *12*, 2557. [CrossRef]
9. Settino, J.; Ferraro, V.; Morrone, P. Energy analysis of novel hybrid solar and natural gas combined cycle plants. *Appl. Therm. Eng.* **2023**, *230*, 120673. [CrossRef]
10. Kotas, T.J. *The Exergy Method of Thermal Plant Analysis*; Butterworths: London, UK, 2012.
11. Gogoi, T.K.; Lahon, D.; Nondy, J. Energy, exergy and exergoeconomic (3E) analyses of an organic Rankine cycle integrated combined cycle power plant. *Therm. Sci. Eng. Prog.* **2023**, *41*, 101849. [CrossRef]
12. González, E.V.T.; Leyte, R.L.; Méndez, H.D.L.; Pereyra, M.S.; García, J.J.A. Exergoeconomic analysis of a triple-level pressure combined cycle with supplementary firing. In Proceedings of the ASME Turbo Expo 2018: Turbomachinery Technical Conference and Exposition, Oslo, Norway, 11–15 June 2018.
13. Calise, F.; d'Accadia, M.D.; Libertini, L.; Vicidomini, M. Thermoeconomic analysis of an integrated solar combined cycle power plant. *Energy Convers. Manag.* **2018**, *171*, 1038–1051. [CrossRef]
14. Mohammadi, A.; Kasaeian, A.; Pourfayaz, F.; Ahmadi, M.H. Thermodynamic analysis of a combined gas turbine, ORC cycle and absorption refrigeration for a CCHP system. *Appl. Therm. Eng.* **2017**, *111*, 397–406. [CrossRef]
15. Ibrahim, T.K.; Mohammed, M.K.; Awad, O.I.; Abdalla, A.N.; Basrawi, F.; Mohammed, M.N.; Najafi, G.; Mamat, R. *A Comprehensive Review on the Exergy Analysis of Combined Cycle Power Plants*; Elsevier Ltd.: Amsterdam, The Netherlands, 2018. [CrossRef]
16. Pacheco-Reyes, A.; Saucedo-Velázquez, J.; Gutiérrez-Urueta, G.L.; Rivera, W. A Novel Cogeneration System for the Simultaneous Production of Power and Cooling Operating with Geothermal Energy: A Case Study in La Primavera, Jalisco, México. *Resources* **2025**, *14*, 22. [CrossRef]
17. Mohammadi, A.; Ashouri, M.; Ahmadi, M.H.; Bidi, M.; Sadeghzadeh, M.; Ming, T. Thermoeconomic analysis and multiobjective optimization of a combined gas turbine, steam, and organic Rankine cycle. *Energy Sci. Eng.* **2018**, *6*, 506–522. [CrossRef]
18. Oko, C.O.C.; Njoku, I.H. Performance analysis of an integrated gas-, steam- and organic fluid-cycle thermal power plant. *Energy* **2017**, *122*, 431–443. [CrossRef]
19. Gu, H.; Cui, X.; Zhu, H.; Si, F.; Kong, Y. Multi-objective optimization analysis on gas-steam combined cycle system with exergy theory. *J. Clean. Prod.* **2021**, *278*, 123939. [CrossRef]
20. de Electricidad, C.F. *Central Termoeléctrica de Ciclo Híbrido del Valle de México*; Prontuario de Datos Técnicos: Mexico City, Mexico, 1994; pp. 1–257.
21. Méndez-Cruz, L.E.; Gutiérrez-Limón M, Á.; Lugo-Leyte, R.; Sales-Cruz, M. Thermodynamic Optimization of Trigeneration Power System. *Energies* **2024**, *17*, 3048. [CrossRef]
22. Lugo-Leyte, R.; Salazar-Pereyra, M.; Bonilla-Blancas, A.E.; Lugo-Mendez, H.D.; Ruíz-Ramírez, O.A.; Toledo-Velázquez, M. Exergetic Analysis of Triple-Level Pressure Combined Power Plant with Supplementary Firing. *J. Energy Eng.* **2016**, *142*, 05016001. [CrossRef]

Disclaimer/Publisher's Note: The statements, opinions and data contained in all publications are solely those of the individual author(s) and contributor(s) and not of MDPI and/or the editor(s). MDPI and/or the editor(s) disclaim responsibility for any injury to people or property resulting from any ideas, methods, instructions or products referred to in the content.